XFEM modelling of degradation-permeability coupling in complex geomaterials

B. Sonon[1], B. François[1], A.P.S. Selvadurai[2], T.J. Massart[1,*]

[1] Building, Architecture and Town Planning CP 194/2, Université Libre de Bruxelles (ULB), Avenue F.D. Roosevelt 50, 1050 Brussels, Belgium
[2] Department of Civil Engineering and Applied Mechanics, McGill University, 817 Sherbrooke Street West, Montreal, Canada, H3A 2K6
* Corresponding author: thmassar@ulb.ac.be

Abstract The theory of poromechanics is widely used to examine problems in the environmental geosciences. In classical poromechanics, the material parameters such as the elastic stiffness or the permeability are assumed to remain constant. The porous fabric can, however, experience micromechanical processes that can lead to alterations in the stiffness and fluid transport characteristics. Experiments on rocks indicate permeability increases even at deviatoric stress states well below peak stress levels, which can contribute to errors in predicting the progress of transient phenomena. This paper presents a multi-scale approach for investigating permeability evolution in a heterogeneous geomaterial. The complex microstructure of geomaterials is modelled using a level set-based extended finite element description (XFEM) that allows uncoupling the meshing operations from the presence of the fine scale material interfaces. A dedicated tool for the generation of representative volume elements based on similar concepts is exploited. Fine scale plastic constitutive laws are used to model the progressive mechanical degradation under stress. The local (fine-scale) permeability evolution can then be coupled to the local plastic dissipation quantities. These fine-scale developments are combined with a versatile computational homogenization technique to upscale mechanical and transport properties corresponding to heterogeneous microstructures. Using this procedure, the effect of progressive degradation on the averaged permeability properties of geomaterials is investigated. These procedures are illustrated by estimating the variation of permeability with the confining pressures and deviatoric stresses applied in triaxial testing.

Keywords Mechanical Degradation, Degradation-induced permeability, Level Set functions, XFEM modelling

1. Introduction

Heterogeneous geomaterials possess complex microstructures. The computational homogenisation of such microstructures requires specific tools to take this complexity into account, both from the point of view of the availability of representative volume elements, and from the point of view of the discretisation technique. This paper presents a level set-based extended finite element description (XFEM), that allows uncoupling the meshing operations from the modelling of the fine scale material interfaces. A dedicated tool for the generation of representative volume elements based on similar concepts is also exploited. Fine-scale plastic constitutive laws are used to model the progressive mechanical degradation under stress. The local (fine-scale) permeability evolution is assumed to be coupled to the local plastic dissipation. Using this procedure, the effect of progressive degradation on the averaged permeability properties of geomaterials is investigated. These procedures are illustrated by estimating the alteration of permeability with the confining pressures and deviatoric stresses applied in triaxial testing.

2. Computational homogenisation of mechanical and transport properties

The upscaling framework described in detail in [1] can be used to extract the homogenised behaviour of a heterogeneous material, starting from its microstructure. The essential features of this approach are summarized below. For completeness, a detailed derivation of the averaging relationships can be found in [1] and references therein.

2.1. Averaged mechanical response of a RVE

The averaged mechanical properties of a heterogeneous material can be deduced by loading a RVE containing the main microstructural features of the material, and solving the corresponding equilibrium problem. When a macroscopic strain $\mathbf{E}$ is applied to a RVE, the displacement of a point inside the RVE is given by

$$\vec{u}(\vec{x}) = E.\vec{x} + \vec{u}_f(\vec{x}) \tag{1}$$

where $\vec{x}$ is the position vector within the RVE and $\vec{u}_f$ is a fluctuation field caused by the heterogeneity of the material. Assuming that the macroscopic strain is the volume average of the fine-scale strain field ε resulting from the above equation, and accounting for a periodic fluctuation, the Hill-Mandel condition (energy equivalence between the fine-scale and macroscopic descriptions)

$$\Sigma : \delta E = \frac{1}{V}\int_V \sigma : \delta\varepsilon \, dV \tag{2}$$

implies that the macroscopic stress tensor is obtained as the volume average of the microstructural stress tensor. Considering the periodicity of the fluctuation field, the macroscopic stress tensor can next be identified based on the cell tying forces at nodes controlling the macroscopic loading as

$$\Sigma = \frac{1}{V}\int_V \sigma \, dV = \frac{1}{V}\sum_{a=1}^{4} \vec{f}^{(a)}\vec{x}^{(a)} \tag{3}$$

where the summation spans the nodes controlling the RVE loading. Any type of material behaviour can be postulated at the fine scale, and the periodicity of the microfluctuation field can be enforced by homogeneous linear connections between corresponding faces. In a three-dimensional body, four controlling points (denoted 1 to 4 in Fig. 1a) are used to apply the macroscopic stress or deformation modes of the boundary of the RVE, provided identical meshes are used on the opposite faces of the RVE.

The RVE equilibrium problem under the macroscopic stress loading is then solved by imposing forces $\vec{f}^{(a)}$ at the controlling points, which represent the action of the neighboring continuum on the RVE. The displacements of the controlling points, energetically conjugated to the imposed controlling forces, can be used to extract the macroscopic strain.

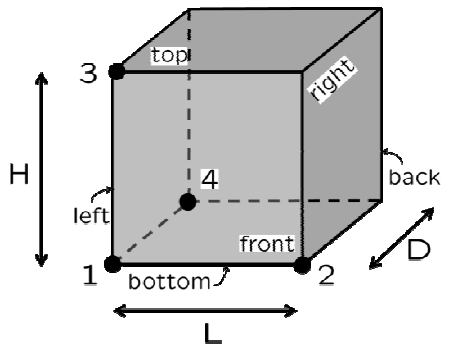

Figure 1. Control points for macroscopic quantities control on a RVE for upscaling principles

2.2. Averaged permeability of a RVE

The homogenised permeability for a given local permeability distribution within the RVE can be evaluated using an upscaling scheme similar to the one developed for heat conduction in [2]. For fluid flow, the mass conservation equation at the scale of the components has to be solved. Expressing the fine scale flux is expressed in terms of the local permeability distribution $K_m(\vec{x})$ and with a fluid of dynamic viscosity μ, mass conservation reads

$$\vec{\nabla}_m \left(-\frac{K_m(\vec{x})}{\mu} \vec{\nabla}_m p_m \right) = 0 \tag{4}$$

A periodic fluctuation $p_f(\vec{x})$ of the pressure field is assumed [1,2] to describe the pressure variation inside the RVE according to

$$p_m(\vec{x}) = p_m^k + \vec{\nabla}_M p_M . \left(\vec{x} - \vec{x}^k \right) + p_m(\vec{x}) \tag{5}$$

where $\vec{\nabla}_M p_M$ is the macroscopic pressure gradient to be applied in an average sense on the RVE, and where p_m^k is the pressure of an arbitrary point in the RVE. An averaging relation for the pressure gradient is required as

$$\vec{\nabla}_M p_M = \frac{1}{V} \int_V \vec{\nabla}_m p_m dV \tag{6}$$

Assuming the periodicity of the pressure field fluctuation and using the Green-Gauss theorem, the average of the fine-scale pressure gradient can be expressed as

$$\frac{1}{V} \int_V \vec{\nabla}_m p_m dV = \vec{\nabla}_M p_M + \frac{1}{V} \oint p_f \vec{n} \, dS \tag{7}$$

With the periodicity of $p_f(\vec{x})$, the last integral of this relationship vanishes and the relationship prescribing the consistency between the macroscopic and fine scale pressure gradients is satisfied. In a computational treatment, the periodicity constraint on the pressure fluctuation field requires that relationships of the form

$$p_m^S - p_m^M = \vec{\nabla}_M p_M . (\vec{x}^S - \vec{x}^M) \tag{8}$$

be satisfied between the master M and slave S nodes of opposite faces of the RVE. An additional averaging relationship is used to impose consistency between scales of the product of the pressure gradient by the flux

$$\vec{\nabla}_M p_M . \vec{q}_M = \frac{1}{V} \int_V \vec{\nabla}_m p_m . \vec{q}_m \, dV \tag{9}$$

Combining the pressure gradient averaging with this relationship, it can be shown that the macroscopic flux is automatically obtained as the RVE average of the fine-scale fluxes [2]

$$\vec{q}_M = \frac{1}{V} \int_V \vec{q}_m \, dV \tag{10}$$

Details of the derivation of this last averaging relationship can be found in [1]. The constraints on the pressures at the boundary can be enforced using control nodes to apply the macroscopic pressure gradients to the RVE. The averaged permeability tensor of the RVE can be identified from the link between the applied macroscopic pressure gradient and the fluxes developing as a reaction

to them. At equilibrium, the discretized system of equations for the transport problem can be condensed at the control nodes

$$q_{m_n}^{(a)} = \sum_{b=1}^{4} k_{disc}^{(ab)} \left(\nabla_j p \; x_j\right)^{(b)} \tag{11}$$

where $k_{disc}^{(ab)}$ results from the condensation of the entire RVE stiffness values. Using periodicity, the averaged flux is obtained from the 'reaction' fluxes at the controlling nodes as

$$q_{M_i} = \frac{1}{V} \oint_S q_{m_n} x_i dS = \frac{1}{V} \sum_{a=1}^{a=4} q_{m_n}^{(a)} x_i^{(a)} \tag{12}$$

Upon substitution of the two previous relationships, one identifies the (averaged) permeability as

$$K_{M_{ij}} = \frac{\mu}{V} \sum_{a=1}^{a=4} \sum_{b=1}^{b=4} x_i^{(a)} k_{disc}^{(ab)} x_j^{(b)} \tag{13}$$

As in the mechanical case, any modelling choice (constitutive laws, discretisation technique) can be adopted for the fine-scale modelling.

3. Representative volume element generation

The RVE generator tool is mainly designed based on distance fields and level set functions as presented in [3] for 2D RVEs, and extended in [4] for 3D simulations. A random distribution of inclusions is first generated, which is subsequently morphed to produce a grain-like structure.

3.1. Inclusion packing

The inclusion packing is the first step of the RVE generation method that gives the basis for the microstructural spatial arrangement. It allows incorporating prescribed volume fractions and/or grain size distributions as input parameters. The geometry used for the shape of inclusions is arbitrary and can be randomly generated through a parameterization, or explicitly defined from existing data (e.g. in order to use data from Computed X-Ray Tomography).

The problem of filling a container with a given volume fraction of inclusions while respecting prescribed size distributions and grain shapes is achieved here using a sequential addition of inclusions, improved by the use of distance fields. In the classical RSA algorithm, each loop generates randomly a trial position in the RVE for the next inclusion to be added. This inclusion is then verified to ensure no interpenetration with previously added inclusions when placed at the trial position, in which case it is rejected and another trial position is generated. Costly computational operations (overlap and distance evaluation) are required at each trial, but few trials lead to a successful inclusion addition, especially when dense packing must be reached.
This original sequential addition methodology can be dramatically improved using distance fields. Instead of a purely random trial position, a set of discrete positions satisfying a priori the non-overlapping and neighboring distance conditions is used to select new inclusion locations. This set is built using the nearest neighbor distance function $LS_1(x)$ (see Fig. 2a) which is maintained on a structured grid of points x_n at each inclusion addition. The radius *r* of the smallest enclosing circle (or sphere) of the new inclusion is used as an indicator of its size.

The positions on the grid leading to overlap with existing inclusions can be excluded for the random inclusion positions by allowing selection only among the points satisfying the condition (Fig.2a)

$$LS_1(x_n) > r \tag{14}$$

This allows the addition of a new inclusion at each trial, and the generation cost is therefore not linked to any probability relative to the actual density, but rather to the number of added inclusions. Additional neighboring distance conditions can be enforced using $LS_1(x)$ such as for instance

$$nn_{min} + r < LS_1(x_n) < nn_{max} + r \tag{15}$$

where $nn_{min}$and $nn_{max}$are the minimum and maximum distance imposed from the first neighbor of the added inclusion (Fig. 2a). To increase packing density, the spatial organization has to be optimized by minimizing the distances of the added inclusion to its second nearest neighbor in 2D and its third nearest neighbors in 3D. The corresponding distance functions $LS_2(x_n)$ and $LS_3(x_n)$ are used for this purpose with the same type of condition (Fig. 2b).

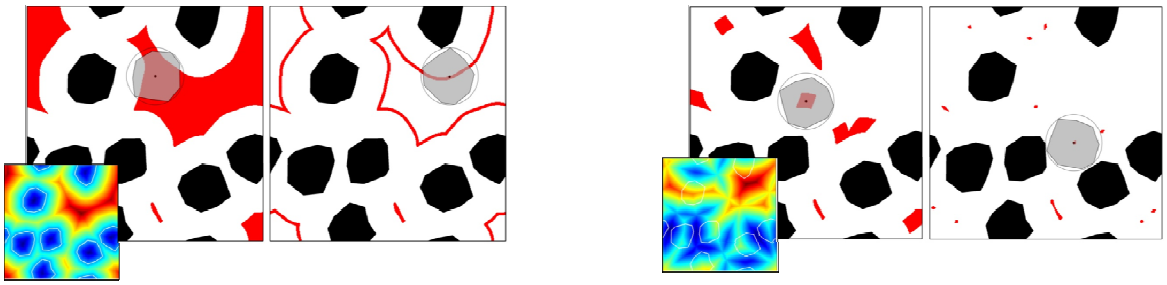

(a) (b)

Figure 2. (a) Non-overlap and first neighbor distance criteria to restrict the random position of the new inclusion to be added (the function $LS_1(\mathbf{x})$ is represented in the insert), (b) First and second neighbor distance criteria to optimize spatial organization to obtain dense packings (the function $LS_2(x_n)$ is represented in the insert)

3.2. Inclusion morphing

Marginal corrections required to adjust the inclusion volume fraction or shapes and more substantial modifications allowing to produce polycrystalline or cellular microstructures motivate the development of a tool enabling the morphing of inclusions once their population is entirely generated by sequential addition. At this stage, the inclusions neighborhood is completely determined and can be used to modify their shape according to inter-inclusion distance rules. A complete expansion of inclusions until vanishing the inter-grain joint thickness allows forming polycrystal-like microstructures.

The morphing technique is strongly based on level set functions. The $LS_1(x_n)$ and $LS_2(x_n)$ functions built during the sequential addition process are used to construct a function $O(x_n)$ that can be contoured to extract updated shapes of the inclusions. The case of complete expansion of inclusions to form a polycrystal morphology is used here to illustrate the methodology. The function

$$O(x_n) = LS_1(x_n) - LS_2(x_n) \tag{16}$$

vanishes at points of equal distance between two nearest inclusions and is negative elsewhere. The zero level set of this function thus determines a Voronoï-like diagram, each cell enclosing an inclusion and points closer to it than to other inclusions. If the initial inclusion distribution is a

dense arrangement of mono-sized spheres, the produced grains are convex and the result is exactly a Voronoï diagram (see Fig. 3a). The use of multi-sized arbitrary shaped polyhedra leads to disordered microstructures (see Fig. 3b). A constant thickness w joint between the grains can be obtained by considering the function $O(x_n) = LS_1(x_n) - LS_2(x_n) + w$.

4. LS-XFEM discretisation for material heterogeneities

The complexity of generating finite element meshes for the generated RVEs motivates the use of an alternative discretisation method. The eXtended Finite Element Method [5], that does not require meshes conforming with the material boundaries, is therefore used. In addition to be defined as an extension of the standard finite element scheme, this method uses the level set formalism to describe the RVE geometry, which allows its seamless integration with the RVE generator.

(a) (b)

Figure 3. (a) convex Voronoï-like cells produced by a circle packing, (b) disordered cells produced by an arbitrary shaped multi-sized inclusion packing

The principle of XFEM is to use a non conforming regular mesh with additional degrees of freedom related to additional shape functions (denoted the enrichment) introducing the strain jumps induced by material heterogeneities. This treatment, concentrated on finite elements intersected by a material interface (e.g. inclusion/matrix boundary), uses signed distance functions to construct the enrichment and to subdivide elements by material at the stiffness integration stage. The interpolation of each displacement field components therefore reads

$$u_{XFEM}(x) = \sum_i N_i(x)\, d_i + \sum_j N_j(x)\, \Psi(x)\, a_j \tag{17}$$

where the first term represents the usual finite element polynomial interpolation containing the standard shape functions as a partition of unity. The second term introduces the XFEM enrichment with a_j the additional unknowns and $\Psi(x)$ the enrichment functions. For heterogeneous materials, the LS_1 level set (distance) function was shown to introduce the required strain jump at the material boundary. This principle is illustrated in Fig. 4 for the 1D case.
Likewise, the pressure field within the heterogeneous microstructure can be described using a similar principle.

$$p_{XFEM}(x) = \sum_i N_i(x)\, p_i + \sum_j N_j(x)\, \Psi(x)\, d_j \tag{18}$$

The XFEM methodology was implemented in a 3D setting, and was coupled with periodic homogenization. The result of the mechanical loading of a RVE can subsequently be used in the

fluid transport simulation, thereby enabling a one-way coupling between the local mechanical degradation of the material and its local permeability.

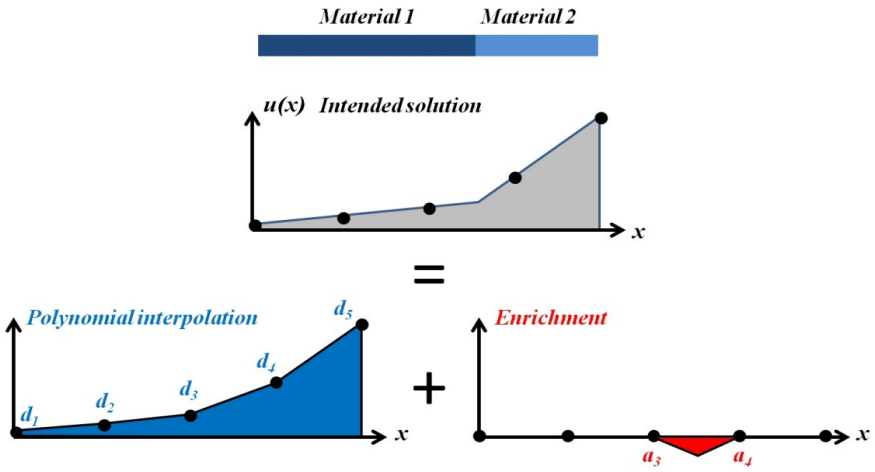

Figure 4. Principle of XFEM enrichment by level set function

5. Application to rock-type materials

The concepts presented previously are now illustrated using two RVEs generated with the tools described in Section 3 and in [4]. The first RVE used for fluid transport homogenisation is produced starting from an initial distribution of elongated inclusions that are subsequently morphed into grains separated by joints. Considering the aspect ratio of the grains, if different permeability properties of the constituents are selected, the resulting average permeability should be anisotropic, as will be illustrated in Section 5.1. The second RVE contains grains without any preferential orientation. The evolving macroscopic permeability resulting from the local plasticity-induced permeability evolution in the joints is analysed in Section 5.2.

5.1. Averaged anisotropic permeability properties

As a first illustration of the proposed level set based homogenisation of heterogeneous materials, the permeability of a anisotropic grain-based material is considered. An anisotropic RVE is generated with a 69% volume fraction of grains (Fig. 5). A grain permeability $k_{grains} = 10^{-13}m^2$ is used, while the joints are assumed 10 times more permeable ($k_{joints} = 10^{-12}m^2$). Since the inclusions are parallel and elongated along the vertical direction, the macroscopic averaged vertical permeability should be higher than for the transverse directions. This is indeed the case as the obtained permeability properties read

$$k_{vertical} = 3\ 10^{-13}m^2 \text{ and } k_{horizontal} = 2{,}3\ 10^{-13}m^2$$

This is further illustrated in Fig. 5 where the fluid flow is illustrated for a unit pressure gradient along the horizontal and vertical directions. As can be seen the preferential orientation of the inclusions clearly favors the fluid flow along the vertical direction, leading to a higher vertical permeability.

5.2. Plasticity-induced permeability evolution in a triaxial test

The coupling between the local mechanical degradation and the fluid transport properties is

illustrated based on a RVE made of grains and large joints with a grain volume fraction of 58%, and subjected to triaxial loading. The RVE is assumed to have dimensions of 10 mm along each direction.

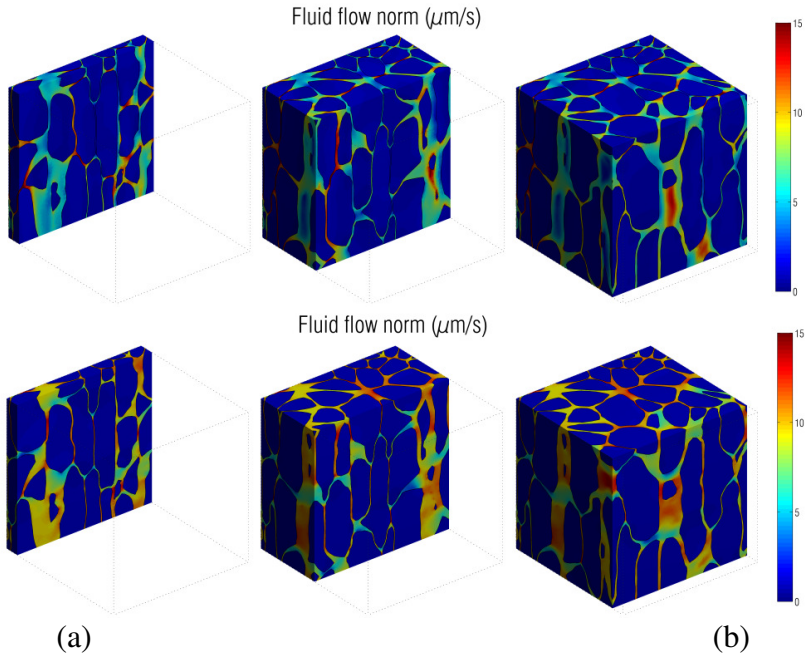

Figure 5. Norm of flow vector for (top) horizontal pressure gradient and (bottom) vertical pressure gradient in anisotropic medium

The grains do not present any preferential orientation as illustrated in Fig. 7. They are assumed purely elastic, whereas a plastic behaviour is assumed in the joints (${}^4H$ is the 4th order elasticity tensor)

$$\sigma = {}^4H : \left(\varepsilon - \varepsilon^{pl}\right) \tag{19}$$

with a Drucker-Prager criterion and an associated flow rule

$$f(p,q) = q - Ap - s(\kappa) \qquad \text{and} \qquad d\varepsilon^{pl} = d\kappa \frac{\partial f}{\partial \sigma} \tag{20}$$

with

$$p = \frac{I_1}{3}$$
$$q = \sqrt{3J_2}$$

where I_1 and J_2 are respectively the first invariant of the stress tensor and the second invariant of the stress deviator. The initial A and s can be expressed as a function of the cohesion c and of the friction angle φ of the material as

$$s = \frac{6c\cos\varphi}{3-\sin\varphi}, \qquad A = \frac{6\sin\varphi}{3-\sin\varphi} \tag{21}$$

To avoid numerical difficulties often met with perfect plasticity, a linear evolution of the yield limit with the plastic strain is introduced through

$$s = s_0 + s_1\kappa \tag{22}$$

Assuming a dilatant behaviour of the joints as defined by an associated plastic flow rule, the volumetric plastic strain increases during the deviatoric loading phase. This increase is used to update the local permeability in plastified joints according to

$$k = k_0\left(1 + B\varepsilon_{vol}^{pl}\right) \tag{23}$$

The set of parameters used in the computations is defined in Table 1. The applied loading follows a typical triaxial test with a strong confinement. A confinement of 100 MPa is first applied in all directions, followed by an increased of the axial stress, the other stress components remaining fixed. This high confining stress is used to avoid any convergence problem in the mechanical problem, and to keep the local strain distribution consistent with a small strain description.

Table 1. Material parameters used in mechanical and fluid transport homogenisation

Material	E	ν	c	φ	s_1	k_0	B
	GPa		MPa	°	GPa	(m²)	
Grains	60	0.1	-	-	-	10^{-13}	0
Joints	30	0.3	40	17	1	10^{-13}	5.10^4

Based on these material and loading parameters, the simulation of the triaxial test is performed. Fluid transport homogenisation is then performed for the mechanical degradation states of the RVE corresponding to successive deviatoric stress levels. The mechanical response of the RVE is depicted in Fig. 6a.

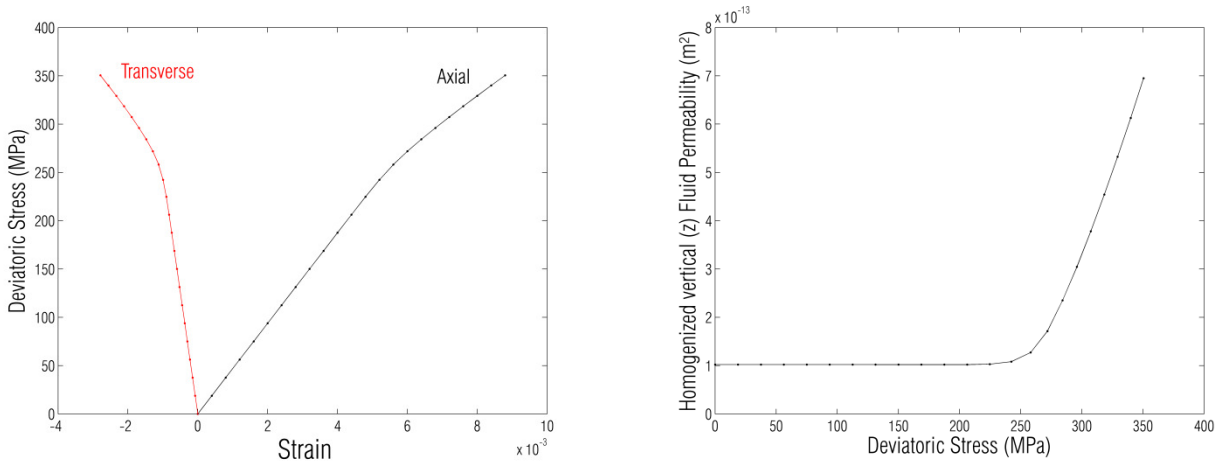

(a) (b)

Figure 6. Homogenised response of the RVE: (a) Mechanical response under triaxial conditions depicting the average deviatoric stress applied as a function of the axial and transverse strains, (b) Axial permeability evolution as a function of the applied deviatoric stress

The corresponding vertical averaged permeability evolution as a function of the deviatoric stress is depicted in Fig. 6b. A permeability increase of almost one order of magnitude is obtained based on the chosen value of the parameter B for the strong confinement applied (100 MPa). The volumetric strain distribution, that directly controls the local permeability evolution inside the RVE, is depicted in Fig. 7. As can be noted from these plots, local permeability can be magnified by a factor up to 500 at a macroscopic deviatoric stress of 350 MPa. The averaged permeability increase for the RVE however remains more restricted as a result of the absence of continuous pathways with high local permeability values inside the microstructure.

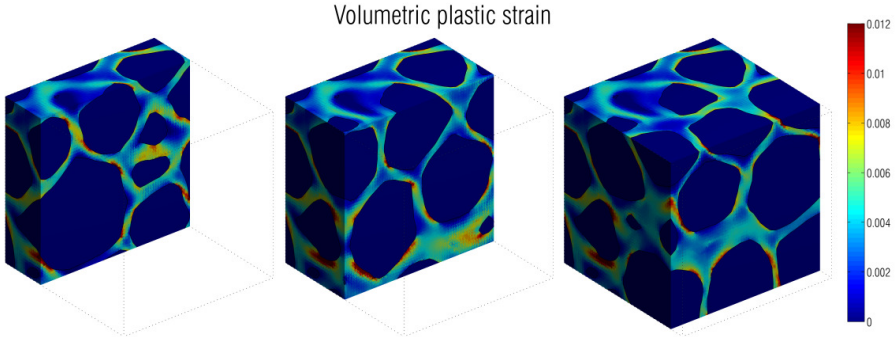

Figure 7. Local volumetric strain distribution inside the RVE at a deviatoric stress of 350 MPa

6. Concluding remarks

Based on the results presented, XFEM discretisation techniques can be efficiently combined with the proposed RVE generation approach to investigate the permeability and mechanical properties of heterogeneous geomaterials. From a fluid transport perspective, this modelling tool could be used in order to identify microstructural features responsible for average (fixed) permeability properties of rocks, in combination with kridging type approaches combined with surface permeability experimental tests [6].

With respect to stress induced permeability evolution, a moderate increase of permeability was obtained as a result of local plastic degradation. Complementary investigations should be performed to analyse the confinement dependency of the permeability evolution, as well as to compare quantitatively such computational results with experimental data. Further developments could incorporate cracking in addition to the plastic dissipation mechanisms contributing to the local permeability evolutions, as well as more advanced plasticity formulations.

Acknowledgements

The first author gratefully acknowledges F.R.S-FNRS Belgium for funding through the FRIA grant 5.0.011.12.F. The Marie Curie International Outgoing fellowship supporting the MULTIROCK project and funded by EU is also acknowledged by the third and last authors.

References

[1] T.J. Massart, A.P.S. Selvadurai, Stress-induced permeability evolution in a quasi-brittle geomaterial, J. Geophys. Res., 117 (2012) B07207.
[2] I. Ozdemir I, W.A.M. Brekelmans, M.G.D. Geers. Computational homogenization for heat conduction in heterogeneous solids. Int. J. Numer. Meth. Engng. 2008; 73:185-204.
[3] B. Sonon, B. François, T.J. Massart, A unified level set based methodology for fast generation of complex microstructural multi-phase RVEs, Comp. Meth. Appl. Mech. Engng., 223-224 (2012) 103-122.
[4] B. Sonon, B. François, T.J. Massart, Generation of complex three-dimensional RVEs for computational homogenisation, In preparation, 2013.
[5] N. Moes, M. Cloirec, P. Cartraud, J.F. Remacle, A computational approach to handle complex microstructure geometries, Comp. Meth. Appl. Mech. Engng. (2003), 192(28-30):3163-3177.
[6] A.P.S. Selvadurai, P.A. Selvadurai, Surface permeability tests: experiments and modelling for estimating effective permeability, Proc. R. Soc. A (2010), 466:2819-2846